



The simulation of morphology of dissimilar copper–steel electron beam welds using level set method

I. Tomashchuk*, P. Sallamand, J.M. Jouvard, D. Grevey

Laboratoire Interdisciplinaire Carnot de Bourgogne, UMR 5209 CNRS-Université de Bourgogne, 12 rue de la Fonderie, F-71200 Le Creusot, France

ARTICLE INFO

Article history:

Received 16 November 2009
Received in revised form 16 March 2010
Accepted 25 March 2010
Available online 21 April 2010

Keywords:

Finite element method
Level set method
Dissimilar welding
Heat transfer
Convection

ABSTRACT

In present work, the simulation of morphology and velocity field in dissimilar electron beam welds formed between the metals with limited solubility is described by the example of copper–stainless steel couple. Finite element software COMSOL Multiphysics 3.5 has been employed due to its flexibility in solving of coupled multiphysical problems.

The domination of horizontal flows allows reducing the model to two dimensions. Level set method has been used to determine the position of the interface between immiscible components basing on coupled heat transfer and fluid flow pseudo-stationary solution.

The evolution of the shape, fluid flow and mixing pattern in function of operational parameters has been demonstrated. The simulated morphology is shown to be in accordance with experimental results: global composition and morphology of the welds.

© 2010 Elsevier B.V. All rights reserved.

1. Introduction

The quality of dissimilar welds is strongly depending on distribution of elements in melting pool. Numerical modeling of mixing process between the components allows better understanding the way of weld formation and the influence of operational parameters on final weld properties. Computational modeling of dissimilar welding has been the object of scientific interest over past few years. There are only several articles dedicated to convection and mass transfer models in dissimilar welds: modeling of turbulent convection in copper–nickel laser beam joint by means of unsteady Reynolds Averaged Navier–Stokes simulation [1] and of dissimilar friction stir welding using the finite elements method-based software [2,3].

The particular feature of copper–steel couple is the limited solubility of copper and iron and the absence of any intermetallic compounds [4]. Due to high thermal gradients and short thermal cycle during electron beam welding these materials when melted coexist without complete dissolving.

We have been interested to create a model that allows reproducing and previewing of composition and morphology of dissimilar weld which is formed between immiscible metals. During the interaction of high power electron beam with metal material, some part of it evaporates giving place to keyhole-like cylindrical cavity surrounded by melted metal. So, there are two phase changes of interest: solid–liquid and liquid–vapor interfaces, which determine

the geometry of the weld. In case of welding of dissimilar materials, there is also moving liquid–liquid interface, which determines internal morphology of melted zone. The chemical composition of melted zone is determined by position of both solid–liquid and liquid–liquid interfaces.

Finite element method, due to facility to solve nonlinear problems and flexibility of formulations, is often used for modeling of thermal, convective and mechanical phenomena in high power beam processing of materials (for example [5–7]). In present research, the finite element software COMSOL Multiphysics 3.4 has been used. The principal advantage of this modeling package is the possibility to solve complex coupled multiphysics problems. It has already made a good showing in modeling of high power sources interaction with matter (welding [8–10], texturing [11,12], manufacturing [13], etc.).

We have chosen the level set method [14] as appropriate tool to reproduce weld morphology by programming change of physical properties across the moving interface between two materials. The method is often used to solve moving boundary problem between melted and evaporated material in case of homogenous welding [15,16], for modeling of alloys dissolution [17] and phase transformation [18]. Level set method is useful for problems where the computational domain can be divided into two domains separated by an interface. As an interface capturing method, it eliminates the need for special tracking procedures associated with interface tracking methods (as, for example, ALE) and handle large distortions and morphology changes of the interface in a more natural way. Highly robust and accurate method, it is relatively easy in implementation and can accommodate complex interface motions

* Corresponding author. Tel.: +33 03 85 73 10 56.

E-mail address: Iryna.Tomashchuk@u-bourgogne.fr (I. Tomashchuk).

Nomenclature

C_p	heat capacity (J/(kg K))	U_r	relative velocity field (m/s)
d	deflection of keyhole from the line of joint (μm)	v_r	y component of relative velocity field (m/s)
D	keyhole diameter (m)	v_w	welding speed (m/s)
E	relative error of calculated composition	W	weld width (m)
g	gravitational acceleration (m/s^2)	ΔT	smoothing region of Heaviside function for phase change (K)
G_r	Grashof number	$\Delta V_{800\text{ }^\circ\text{C}}$	electromotive force of thermocouple under 800 °C (mV)
h	height of workpiece (m)	β	thermal expansion coefficient (m/K)
I	beam current (mA)	ε	width of moving interface (m)
k	thermal conductivity (W/(m K))	ε_m	emissivity of metallic surface
L	weld length (m)	ϕ	level set function
L_b	average characteristic length of buoyancy convection (m)	φ_{Cu}	real copper amount in melted zone (at.%)
R_e	Reynolds number	φ_{Cu^*}	calculated fraction of melted copper in the melted zone (%)
S_{wp}	the total surface of melted zone, enclosed between melting and vaporization isotherms	γ	reinitialization parameter (m s/kg)
$S_{\phi>0.5}$	the surface occupied by melted copper ($\phi > 0.5$)	η	dynamic viscosity (Pa s)
T	temperature (K)	ν	cinematic viscosity (m^2/s)
T_m	melting temperature (K)	ρ	density (kg/m^3)
T_{vap}	vaporization temperature (K)	σ	Stefan–Boltzmann constant ($\text{W}/(\text{m}^2 \text{K}^4)$)
U_a	acceleration voltage (kV)	$\sigma_{L1/L2}$	surface tension between immiscible phases (N/m)
u, v	x and y components of velocity field (m/s)	θ	angle of beam deflection (°)
U	velocity field (m/s)		

of curves and surfaces on fixed Cartesian grid without having to parameterize these objects or significantly increase theoretical or implementation complexity. The moving interface easily locates, which gives to level set the advantage on often used enthalpy method, which only has an approximate representation of the interface location. We have decided to apply recently appeared (2008) level set application mode of COMSOL Multiphysics software package, which has been introduced as promising and easy to use for description of two-phase flow [19].

2. Experimental part

The composition of dissimilar weld is mostly determined by the position of heat source relatively to joint line. It is known, that electron beam can be deflected from the joint line by magnetic field created by the pair of dissimilar metals [20]. The angle of deflection is a function of acceleration voltage of the beam:

$$\theta \sim \Delta V_{800\text{ }^\circ\text{C}} / U_a^{1/2} \quad (1)$$

where θ : the degree of beam deflection; $\Delta V_{800\text{ }^\circ\text{C}}$: electromotive force of thermocouple under 800 °C and U_a : acceleration voltage of electron beam.

For the couple copper–austenitic stainless steel $\Delta V_{800\text{ }^\circ\text{C}}$ is 5.6 mV [20], which corresponds to weak beam deviation. So the effect is not so pronounced to make joining impossible, but the composition of the weld can change in very large range, as it is shown on Fig. 1.

The intensity of current, considered important enough to obtain full penetration, does not make observable effect on the deflection of electron beam.

A number of 2 mm thick joints of pure copper with AISI 316 austenitic stainless steel have been realized (Table 1). To find out the deviation of beam from the joint line, we have measured the distance between the center of weld stop point (where solidified cavity approximate to keyhole is observable) and the joint line (Fig. 2). We consider the positive values of deviation at the copper side (+d) and negative (−d) at steel side. The EDS analysis shows that below $U_a = 37.5$ kV copper dominates in melting pool (94–95 at.%), and above $U_a = 37.5$ kV, when the deflection is suppressed, the joints are rich in steel.

We should mention that the final position of the keyhole seems to be determined not only by the angle of beam deflection, but also by the difference in physical properties of materials, which brings the additional asymmetry to the system. For example, in case of maximum of acceleration voltage (40 kV) deflection is totally suppressed (joint 6), but the keyhole has a negative deviation. We attribute this to high thermal conductivity of copper, so the keyhole appears in steel which reaches more rapidly the temperature of vaporization.

We have found three principal types of morphology on the horizontal cross-sections of the welds (Fig. 3): rich in copper with a small part of melted steel that forms thin irregular layer between melted pool and solid steel (a); rich in steel, which presents visible solidification waves (b) and mixed, which presents the solidification pattern formed by intersection of copper and steel fluxes (c).

The most important mixing produces in case of joints with centered beam position. The result of superposition of fluxes is visible as complex pattern with a strict repetitively which can be attributed to temporal instability of fluid flow in electron beam welding [21]. Sayegh and Voisin [22] establish the linear dependence between the length of solidification wave and the welding speed. Because of intersection of solidification waves, only back part of the melted pool is observable at the pictures of the welds.

The composition of copper–steel joint makes effect on its quality: joints with small amount of copper are susceptible to intergranular cracking, and copper-rich joints show low value of ultimate tensile strength [23]. The mixed joints with important interweaving of copper and steel domains appeared to have the better mechanical properties (tensile strength ≈ 310 MPa).

We have observed the horizontal cuts on different depth and found that the width and morphology does not change significantly (Fig. 4). That allows us to reduce the model to two dimensions and work only on horizontal cut of the weld.

3. Model description

The position of immiscible zones in the weld pool is determined both by heat transfer and fluid flow. We propose 2D model of horizontal plane of the weld with simple geometry (Fig. 5) where two

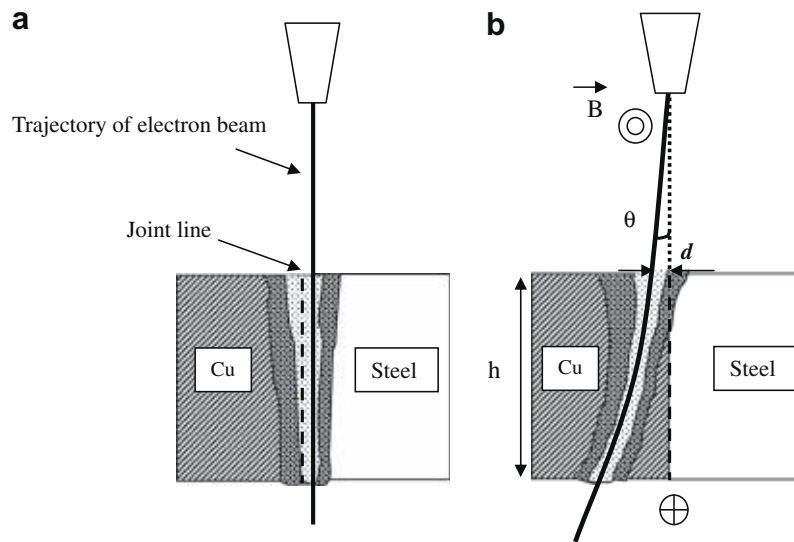


Fig. 1. The scheme of beam deviation on the transversal cut of the joint: absence of deviation under high acceleration voltage (a), appearance of deviation under small acceleration voltage (b).

Table 1

Operational parameters and bulk chemical composition of electron beam welds (where I – beam current, U_a – acceleration voltage, v_w – welding speed, d – resulting deflection of keyhole from joint line).

Weld	I (mA)	U_a (kV)	v_w (mm/min)	d (μm)	Elemental composition (at.%)			
					Cu	Fe	Ni	Cr
1	30	20	200	280	100	0.0	0.0	0.0
2	20	30	200	420	91.3	6.2	1.8	0.7
3	32	25	300	375	95.3	3.3	1.0	0.4
4	25	32	300	380	94.2	4.1	1.2	0.5
5	40	25	600	400	94.5	3.9	1.2	0.4
6	25	40	600	–200	8.8	64.7	19.1	7.3
7	30	37.5	600	–120	52.7	33.6	9.9	3.8
8	35	40	900	0	58.2	29.7	8.8	3.3
9	35	25	300	300	94.1	4.2	1.2	0.5
10	37.5	30	600	600	94.7	3.8	1.1	0.4
11	40	35	900	550	95.1	3.5	1.0	0.4

different materials are represented by two plates and the simplified vapor keyhole as a circle with a diameter D equal to average diameter of electron beam (400 μm). The domains were meshed

with maximal element size of 100 μm . Fine meshing around the keyhole is applied (10 μm).

The initial considerations of the model are:

- only horizontal propagation of phenomena is considered (plane symmetry);
- the energy source is presented as isotherm of vaporization;
- vaporization zone is geometrically imposed;
- no solubility between dissimilar materials;
- no diffusion phenomena on liquid/liquid interface.

The input data for the model are the welding speed (v_w) and the position of keyhole with respect to the plane of joint (d). The physical properties of the materials are presented in Table 2.

3.1. Heat transfer

Differently from the enthalpy formulation, the basic order-parameter method for description of phase change [24,25], our description of melting is based on pseudo-stationary heat equation, which considers only the temperature as the dependent variable, hence no direct relationship between enthalpy and temperature is required.

A pseudo-stationary heat transfer approach has been considered. It reproduces the weld shape which is continuous in time

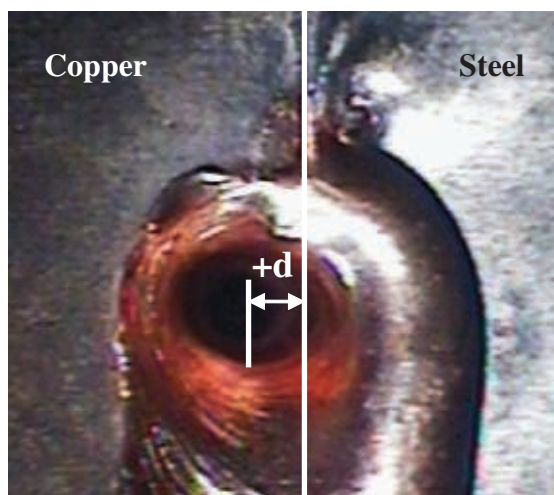


Fig. 2. The measurement of beam deflection at the stop point of the weld.

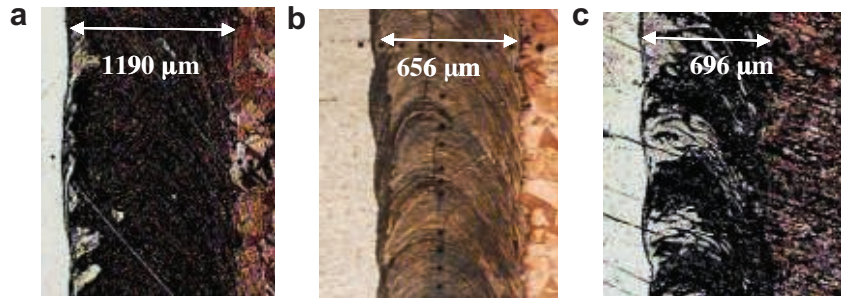


Fig. 3. The solidification patterns on horizontal cuts of the welds: Weld 5 (a), Weld 6 (b), and Weld 7 (c) (copper on the right).

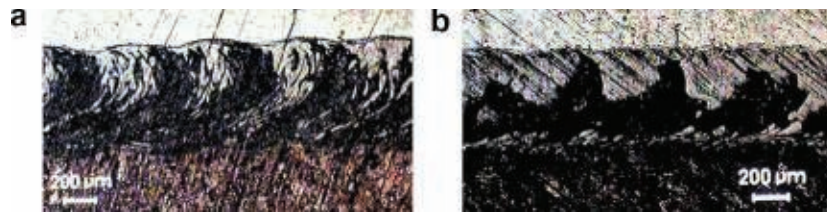


Fig. 4. The morphology of the Weld 7 observed on 400 μm (a) and 1500 μm (b) from the top surface.

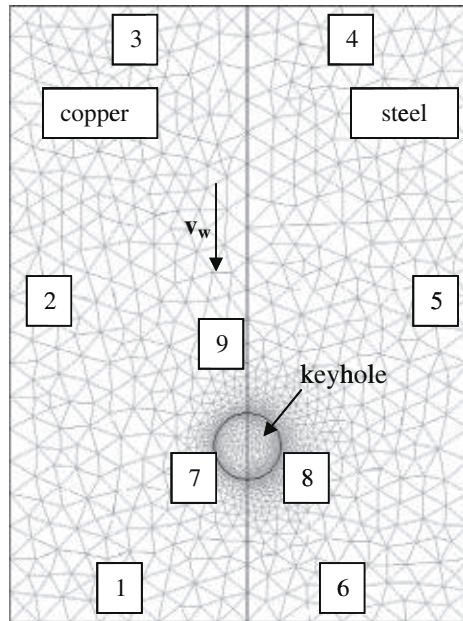


Fig. 5. The geometry of the model.

Table 2
Physical properties of materials used in calculations.

Constant	Unit	Name	Materials	
			Copper	AISI 316L
Fusion temperature	K	T_m	1356	1720
Vaporization temperature	K	T_{vap}	2835	3013
Density (solid)	kg/m ³	ρ_s	8700	7980
Density (liquid)	kg/m ³	ρ_L	7940	7551
Heat capacity (solid)	J/(kg K)	C_{pS}	385	433
Heat capacity (liquid)	J/(kg K)	C_{pL}	350	734
Thermal conductivity (solid)	W/(m K)	k_S	400	8.116
Thermal conductivity (liquid)	W/(m K)	k_L	140	12.29
Dynamic viscosity (solid)	Pa s	η_S	1	1
Dynamic viscosity (liquid)	Pa s	η_L	0.003	0.005

but moving with given constant velocity by introduction of welding speed in heat equation:

$$\rho \cdot C_p \cdot \vec{U} \cdot \vec{\nabla} T + \vec{\nabla} \cdot (-k \cdot \vec{\nabla} T) = 0 \quad (2)$$

where the properties of the materials are given as:

$$k = \begin{cases} k_L, & K > T_m \\ k_S, & T < T_m \end{cases}; \quad \rho = \begin{cases} \rho_L, & K > T_m \\ \rho_S, & T < T_m \end{cases}; \quad C_p = \begin{cases} C_{pL}, & K > T_m \\ C_{pS}, & T < T_m \end{cases} \quad (3)$$

The evolution of materials properties during phase change has been introduced by using of Heaviside smoothing function allowing avoiding the sharp discontinuity, which leads to convergence problems. The real function of temperature, usually having the slow change in solid phase, augmentation in partially melted state and more rapid change in liquid phase, is approximated by two regions corresponding to solid and liquid state, where the average constant value is considered, separated by smoothed region corresponding to phase change interval. This simplification is determined, above all, by the insufficient and divergent literature data on evolution of physical properties in melted metals and alloys. However, this formulation can be easily improved by contributing of empirical or calculated function of temperature corresponding to each phase state. A phase change interval of 50 K is sufficient to obtain stable pseudo-stationary solution.

Our initial hypothesis is that the temperature of the walls of the keyhole is not far from vaporization temperature of materials. The keyhole has been introduced as equivalent heat source having vaporization temperature of corresponding material: boundary 7 has T_{vap} (AISI 316L) and 8 has T_{vap} (Cu). Comparing to energy input provided by electron beam (about 10^{12} W/m²), the energy released by local melting is considered as negligibly small.

The other boundary conditions are (Fig. 5):

- 1 and 6 – ambient temperature considered as 300 K;
- 2 and 5 – radiation heat loss ($\varepsilon_m = 0.4$): $\vec{n} \cdot (-k \cdot \vec{\nabla} T) = \varepsilon_m \cdot \sigma \cdot (T_{amb}^4 - T^4)$;
- 3 and 4 – convection flux: $\vec{n} \cdot (-k \cdot \vec{\nabla} T) = \rho \cdot C_p \cdot \vec{v}_w \cdot \vec{n}$;
- 9 – continuity of energy flux.

3.2. Fluid dynamics

An incompressible, laminar and Newtonian liquid flow is assumed in the weld pool:

$$\begin{aligned} \rho \cdot (\vec{U} \cdot \vec{\nabla} T) \cdot \vec{U} &= \vec{\nabla} \cdot (-\rho + \eta \cdot (\vec{\nabla} \vec{U} + (\vec{\nabla} \vec{U})^T)) \\ \vec{\nabla} \cdot (\rho \cdot \vec{U}) &= 0 \end{aligned} \quad (4)$$

where $\vec{U} = (u, v)$: the global velocity field where u and v are x and y velocity components; $\eta = \begin{cases} \eta_L, & T > T_m \\ \eta_s, & T < T_m \end{cases}$ – the dynamic viscosity of liquid metals. The viscosity of solid has been considered as 1 Pa s which is sufficient to suppress all movement beyond melted zone.

We consider only viscous force in weld pool, because of insignificant importance of natural convection, as Grashof number for this system is inferior to one:

$$G_r = \frac{g \cdot \beta \cdot L_b^3 \cdot (T_v - T_m) \cdot \rho_L^2}{\eta^2} = 0.03 \quad (5)$$

where $L_b = 1/8 L$ [26]: average characteristic length of buoyancy convection and β : thermal expansion coefficient (taken as 2×10^{-5} m/K).

The value of Reynolds number

$$R_e = \frac{v_w \cdot L \cdot \rho_L}{\eta} \quad (6)$$

indicating the flow mode in the weld pool has been found to be 10–30, which corresponds to recirculation flow mode [27].

The boundary conditions are follows: welding velocity is imposed to all external limits, when non-slip condition is applied to keyhole walls.

Resulting velocity field is the superposition of welding speed (the displacement of entire junction) and velocity of liquid metals. Subtracting the welding speed from resulting velocity field, we obtain the relative velocity field \vec{U}_R that corresponds to movements of melted metals relative to keyhole:

$$\vec{U}_R = (v - v_w, u) = (v_r, u) \quad (7)$$

3.3. Movement of liquid/liquid interface

When the resolution of pseudo-stationary heat equation with Heaviside-type functions for materials properties serves to delimitate the melted zone from solid material, level set function serves to delimitate one immiscible liquid phase from another by smoothed interface.

The level set method is a technique to represent moving interface or boundaries using fixed mesh. The movement of liquid/liquid interface between two immiscible metals is given by the equation:

$$\frac{\partial \phi}{\partial t} + \vec{U}_r \cdot \vec{\nabla} \phi = \gamma \cdot \vec{\nabla} \cdot \left(\varepsilon \cdot \vec{\nabla} \phi - \phi \cdot (1 - \phi) \cdot \frac{\vec{\nabla} \phi}{|\vec{\nabla} \phi|} \right) \quad (8)$$

where ϕ : level set function that varies from 0 (steel) to 1 (copper) and is equal to 0.5 at the interface between the materials; ε : the parameter that determines the thickness of the region where ϕ goes smoothly from 0 to 1 (taken as 50 μm , which corresponds to $1/2$ of mesh size) and γ : the mobility parameter that determines the amount of reinitialization of the level set function, that can be specified as a relation between the order of velocity in the system and the interfacial tension between two liquids:

$$\gamma = \frac{|U_R|}{\sigma_{L_1/L_2}} \quad (9)$$

If estimating average velocity of liquid flow about 1 mm/s and considering $\sigma_{L_1/L_2} = 0.2$ N/m [28], the mobility of the interface will be equal to 0.005 m s/kg. \vec{U}_R : velocity field relatively to keyhole.

The boundary conditions are:

- 1, 2 and 7 – $\phi = 0$ (steel domain);
- 5, 6 and 8 – $\phi = 1$ (copper domain);
- 3 and 4 – outflow: $\vec{n} \cdot (\varepsilon \cdot \vec{\nabla} \phi - \phi \cdot (1 - \phi) \cdot \frac{\vec{\nabla} \phi}{|\vec{\nabla} \phi|}) = 0$;
- 9 – initial interface position between copper and steel domains:

$$\vec{n} \cdot (\vec{N}_1 - \vec{N}_2) = 0, \vec{N} = \varepsilon \cdot \vec{\nabla} \phi - \phi \cdot (1 - \phi) \cdot \frac{\vec{\nabla} \phi}{|\vec{\nabla} \phi|} - \phi \cdot \vec{U}_r.$$

The particular advantages of described approach comparing to enthalpy method residue in follows:

1. It allows to reproduce the shape of stationary melted zone by solving of pseudo-stationary heat equation and Navier–Stokes equation basing even on relatively limited data on materials properties.
2. Use of level set method for capturing the interface between immiscible liquid phases allows reproduce the complex motion and easily locate the interface, when the enthalpy method provides only approximative interface position.
3. The possibility to adjust the thickness of liquid/liquid (ε parameter) and solid/liquid interface (dT parameter) allows to obtain accurate solution basing on fixed Cartesian grid.
4. Better convergence and stability of the method allows to solve the problem directly with use of basic direct solver provided by COMSOL Multiphysics.

The limitations of the model residue in:

1. Absence of complete coupling between implicated application modes, which is scarified to diminish the time of calculation.
2. Implicit consideration of surface tension between liquid phases.
3. The impossibility to handle the distribution of intermetallic phases issued from convective–diffusive transport between immiscible regions, which can be done by enthalpy method [29]. However, such phases are absent in discussed system.
4. The model describes only morphology of one weld pool and does not allow recreating repetitive solidification wave patterns. It allows however to reveal the tendencies in morphology of weld pool.

3.4. Solving scheme

We use two step solving scheme: (1) solving of coupled pseudo-stationary heat transfer and fluid dynamics problem with direct UMFPACK solver; (2) solving of level set problem in temporary mode using previously calculated relative velocity field \vec{U}_r with direct temporary UMFPACK solver and the time of calculation given as $t = v_w/L$, where L is a length of melting pool. This approach allows significant reducing of the time of calculation and operative memory required.

As the result, we obtain temperature, velocity and level set function fields. The profile of melting zone has been obtained as superposition of the isotherms T_m^{copper} when $\phi > 0.5$ and T_m^{steel} when $\phi < 0.5$. Level set function field reproduces the horizontal morphology of the weld, but does not give the direct value of proportion between melted components. We have introduced the variable ϕ_{Cu} that is analogous to common copper amount in volume percents:

$$\phi_{Cu} = S_{\phi > 0.5} / S_{wp} \cdot 100\% \quad (10)$$

where $S_{\phi > 0.5}$ is the surface enclosed between the isotherm of T_m^{copper} and liquid/liquid interface (where $\phi > 0.5$) and S_{wp} – the surface

enclosed between melting and evaporating isotherms. As the ratio of atomic mass to density are close for these materials, the difference between atomic and volumic percents is negligible comparing to error of EDS analysis.

4. Results and discussion

The results of calculations, including thermal, velocity and composition fields, has been analyzed to reveal and explain the tendencies in evolution of melted zone morphology in function of welding parameters and to validate the model by comparison with experimental data.

4.1. Thermal field and external morphology of weld pool

The profiles of calculated weld pools have been compared to real shapes of the welds, with special attention to the form of crystallization front after beam pass. The calculated shape of weld pool is given as isotherm line of melting temperature corresponding to one of materials (Fig. 6). The good correspondence between the form of calculated and observed weld pools has been found, which validates our hypothesis that the walls of keyhole have the temperature not far from the vaporization temperature of corresponding metal.

The shape of weld pool is mainly determined by initial position of keyhole. In case of positive deviation (at the copper side), resulting weld pool is large. For negative or insignificant deviation, the thickness is two times smaller because of higher melting temperature of steel and important conductive heat flux in the direction of solid copper. The correspondence of calculated and observed width of weld pools is close to 90% (Fig. 7).

4.2. Convection in the weld pool

We have compared the velocity fields for the joints with different beam deviation (Fig. 8). The color distribution on them corresponds to scalar relative velocity field U_r , created by continuous displacement of keyhole in melted material. The strong recirculation movements have been observed. However, velocity field close

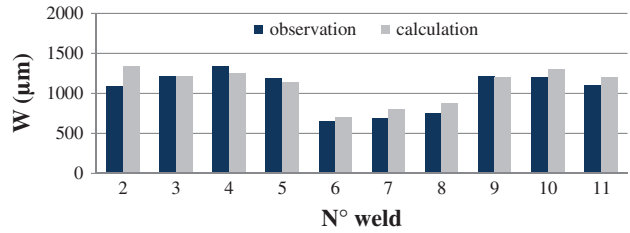


Fig. 7. The correspondence between calculated and observed width of the weld pools.

to back side of keyhole may be not realistic due to the fact that real back profile of keyhole is unknown and may be different from circle.

The evolution of the fluxes situated behind the keyhole with change of beam deviation from the joint line has been investigated (Fig. 9). Weld 6 having maximal negative deflection $d = -200 \mu\text{m}$ has a significant steel-rich flux that flows around the keyhole, when the convection at the copper side is located in negligibly small region. Weld 7 with $d = -120 \mu\text{m}$ present almost symmetric copper and steel fluxes, but steel flux is much extended in the back of melted pool. Weld 8 ($d = 0 \mu\text{m}$) present slow steel flux and copper flux that is four times more rapid. For the welds with big positive deviation (as Weld 5) continuous steel flux is no longer present. We observe two identical copper fluxes, one of which erode steel side and may form a thin layer of liquid steel.

The comparison of u velocities at the plane of joint (Fig. 10) allows understanding the direction of dissimilar fluxes: which of materials enters at the opposite side. All fluxes from copper side to steel side are chosen to have negative u value, and the fluxes from steel to copper side – positive u value. For Weld 6 ($d = -200 \mu\text{m}$), we observe very local and rapid flux from steel into copper before keyhole followed by less rapid opposite flux from copper to steel. The effective length of the interface between melted metals is only about $350 \mu\text{m}$, so there is no significant inflow of copper in melted pool, as it was confirmed by elemental analysis. For mixed joints 7 and 8, local and very rapid flux from steel to copper side before keyhole and important and large flux

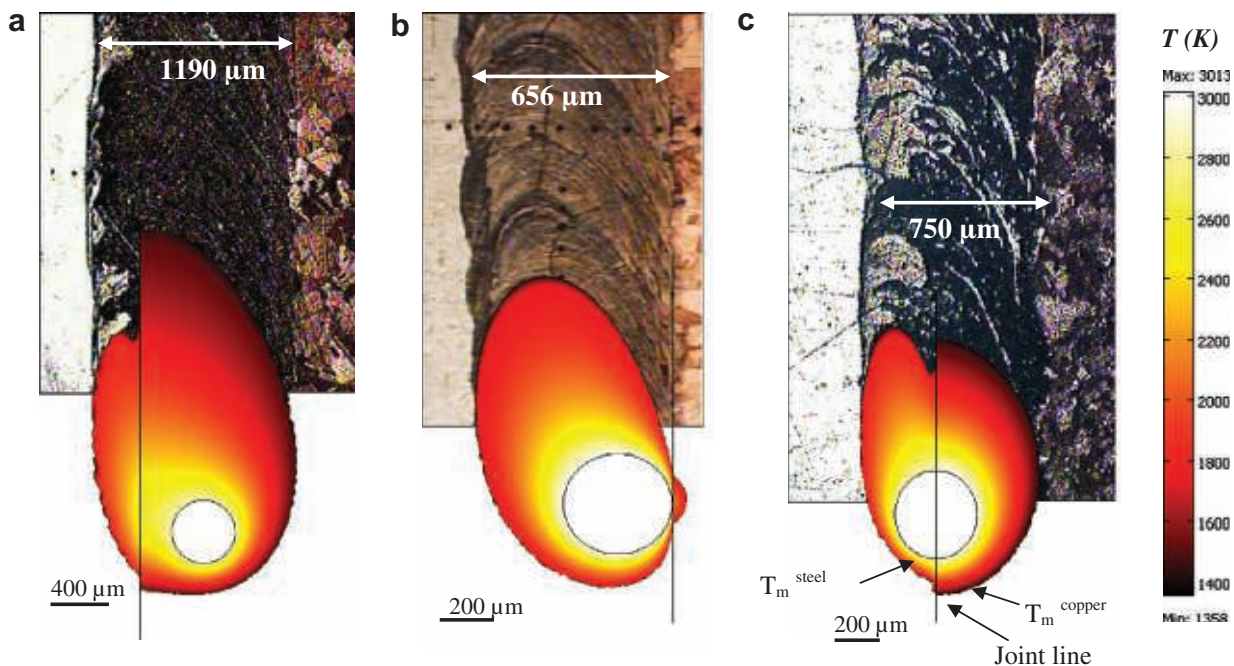


Fig. 6. Comparison between calculated and observed shapes of weld pool: Weld 5 (a), Weld 6 (b), Weld 8 (c) (copper on the right, $D = 400 \mu\text{m}$).

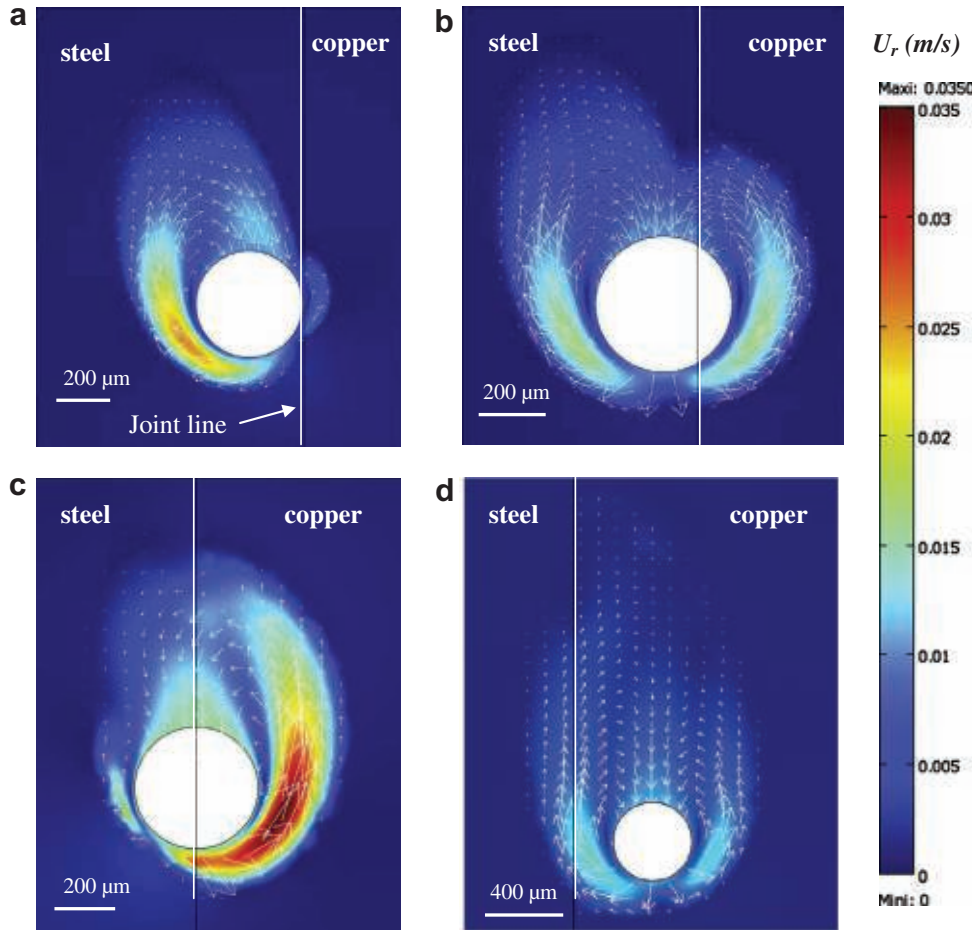


Fig. 8. Relative velocity fields U_r of: Weld 6 ($d = -200 \mu\text{m}$) (a); Weld 7 ($d = -120 \mu\text{m}$) (b); Weld 8 ($d = 0 \mu\text{m}$) (c); Weld 5 ($d = 400 \mu\text{m}$) (d). $D = 400 \mu\text{m}$.

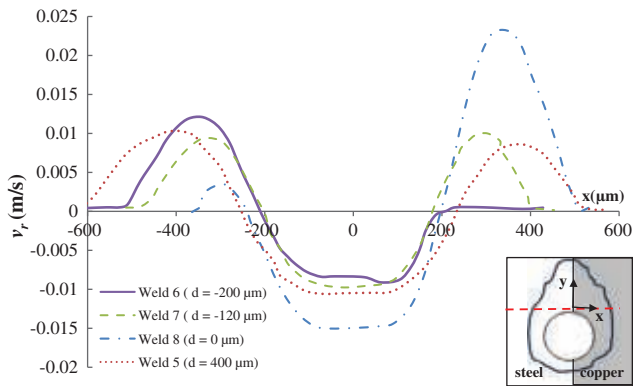


Fig. 9. Distribution of v_r behind the keyhole (zero point is the center of keyhole).

from copper to steel after keyhole have been found. The welds 2, 4 and 5, rich in copper (Fig. 10b), present local rapid flux from copper to steel (that erodes steel surface), and relatively long (about 1 mm) slow flux from steel to copper, which brings steel particles into melted pool. The values of velocity field and so, the efficiency of mixing in the melted pool depend directly on the welding speed.

4.3. Reproduction of joint morphology and composition

The evolution of weld pool morphology has been calculated over the wide range of d (Fig. 11). As it was previously mentioned,

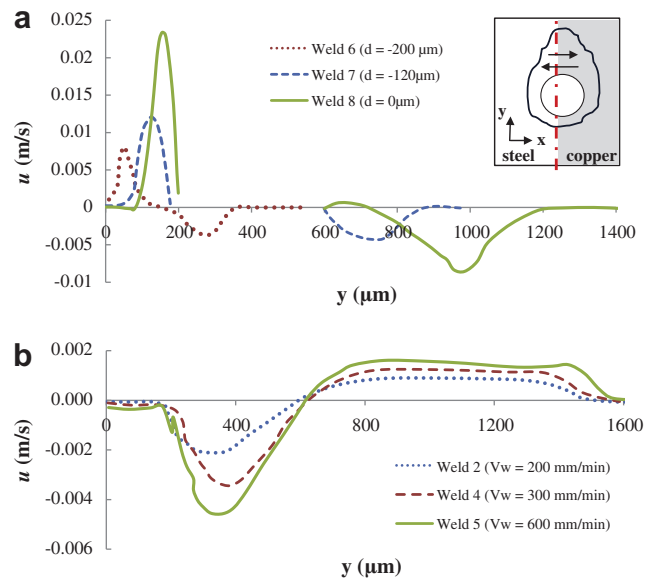


Fig. 10. The velocities perpendicular to joint line: steel-rich (a) and copper-rich welds (b).

beam deflection at steel side has been chosen as negative, and positive at copper side.

Maximal negative deflection under which welding in steel possible is about $-200 \mu\text{m}$. In this case, the keyhole is totally situated

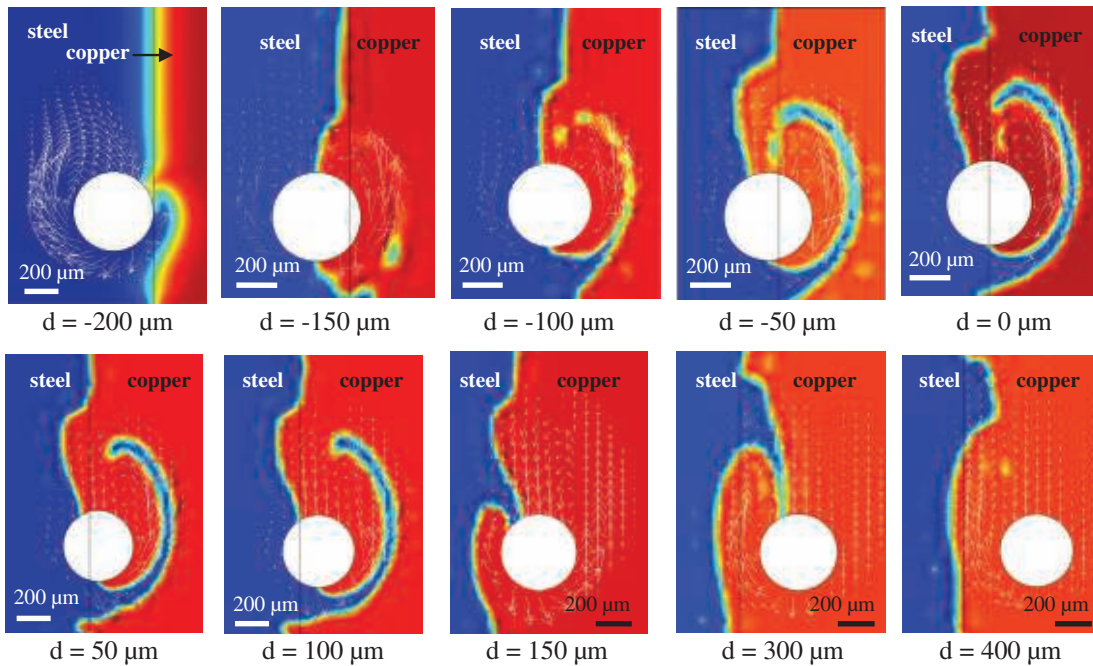


Fig. 11. The evolution of weld morphology under different values of beam deflection ($v_w = 900$ mm/min, $D = 400$ μm).

at steel side, and copper arrives in weld pool only with a small flux of steel that erodes solid copper side. Under deviations from -150 to -100 μm two almost symmetric fluxes (copper and steel) collide behind the keyhole. From $d = -100$ μm to 150 μm, we observe important mixing of components: slow flux of melted steel rounding the keyhole wall, collides with an important flux of melted copper. At the same time, there is a possibility that some part of melted steel can go at the copper side without complete mixing with major copper flow and forming curved steel band in copper medium. Starting from $d = 150$ μm, two fluxes of copper form around the keyhole. One of them erodes solid steel and forms the layer of melted steel which decrease proportionally to growth of beam deviation.

With respect of bulk composition, the joints can be divided on three groups (Fig. 12): (1) $d < -100$ μm, when the keyhole founds mostly at steel side; (2) 100 μm $< d < -100$ μm, when keyhole is situated in both materials which leads to formation of joints with composition close to 50/50; (3) $d < 100$ μm, where the keyhole is situated mostly in copper, and the quantity of melted steel diminish rapidly with progress of negative deviation.

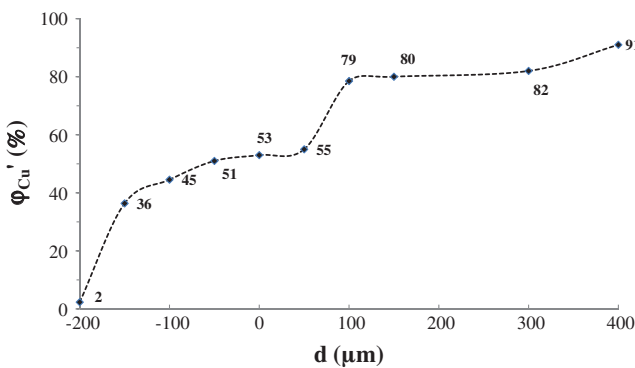


Fig. 12. Average composition of the welds as a function of beam deflection ($v_w = 900$ mm/min).

We have been interested also in influence of welding speed on composition of the welds (Fig. 13). Three values of deflection (-200 , 0 and 400 μm) have been chosen. The welding speed has been varied from 0.3 to 1.2 m/min. It was found that the impact of welding speed on composition depends on with beam deviation: for $d = 0$ and $d = 400$ μm higher welding speed leads to augmentation of copper amount on 25 at.%, when for $d = -200$ μm it remains stable. Such growth of copper amount can be explained by lower melting point and higher thermal conductivity of copper: with augmentation of welding speed, the steel side of weld pool became more and more thin and long, when copper side retains its thickness but gains also in length. For example, for $d = 0$ μm, $v_w = 0.3$ m/min the isotherm of melting at the steel side is situated at the distance of 480 μm from joint line and copper – on 510 μm, when for $v_w = 1200$ mm/min steel side is only of 330 μm, when copper side remains on 500 μm.

The morphology of real welds has been compared to liquid/li-liquid interface position resulting from level set calculation. For

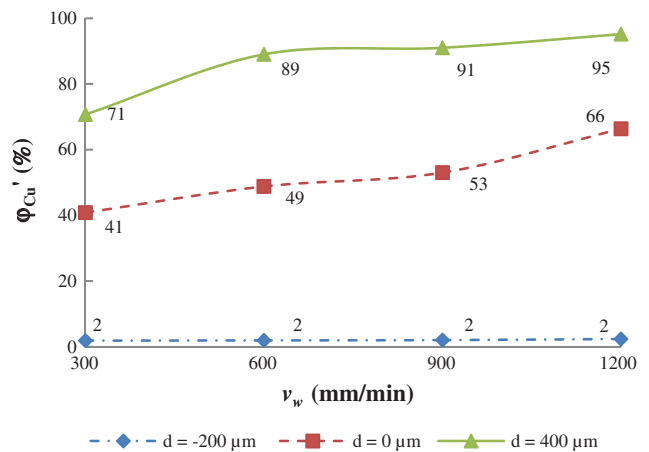


Fig. 13. Average composition of the welds as a function welding speed (for three values of beam deflection).

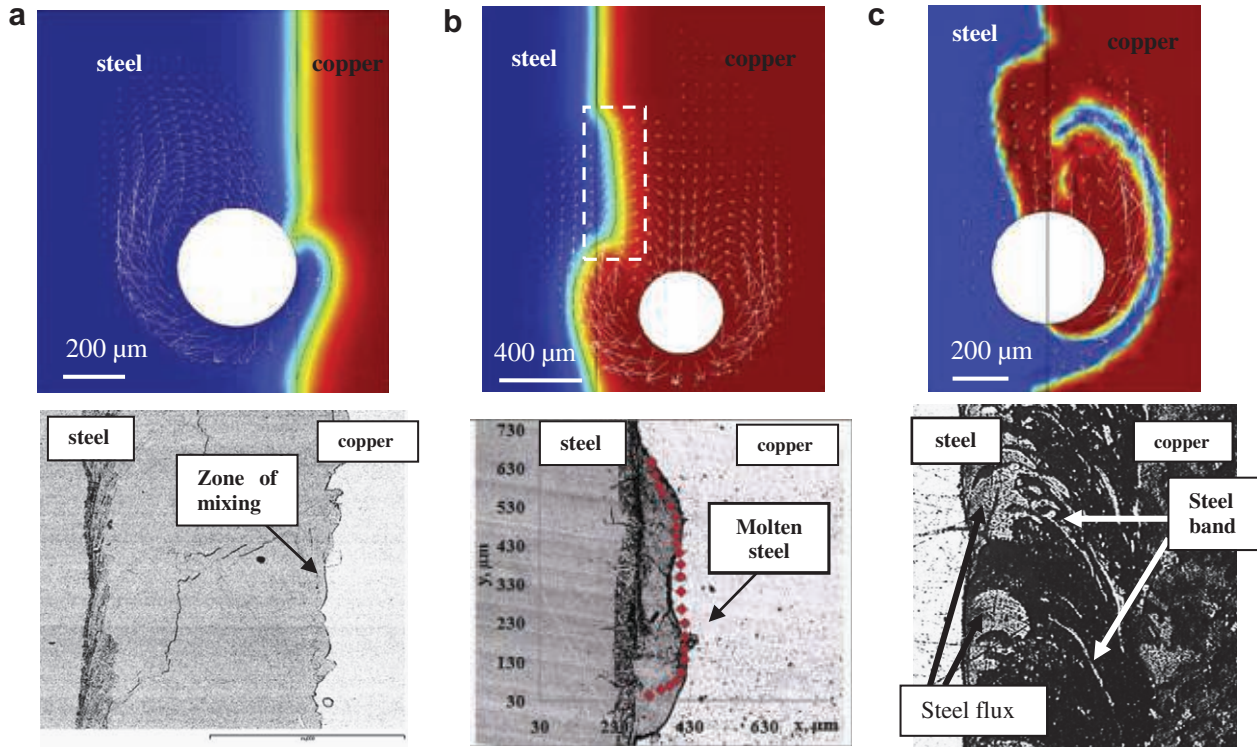


Fig. 14. Comparison of calculated and real morphologies of the welds: (a) Weld 6, (b) Weld 4, (c) Weld 8.

steel-rich and copper-rich joints good correspondence of morphology has been observed: in first case SEM-image reveals thin zone of mixing that corresponds to local copper flux in level set solution (Fig. 14a); in the second case, the satisfactory coincidence has been found for the melted steel film and the calculated interface position (Fig. 14b). For mixed joints (Weld 8) comparison is more complicated because of irregular character of solidification wave content. Nevertheless it is possible to identify several elements of morphology: numerous irregular steel bands formed in copper medium and compact steel flux in copper medium (Fig. 14c).

We have compared calculated fraction of copper ϕ'_{Cu} (%) with real fraction ϕ_{Cu} (at.%) obtained by elemental analysis of real welds (Table 3). The relative error of calculation E has been introduced as:

$$E (\%) = \begin{cases} \frac{\phi_{Cu} - \phi'_{Cu}}{\phi_{Cu}} \cdot 100 & \text{if } \phi_{Cu} > 50\% \\ \frac{\phi'_{Cu} - \phi_{Cu}}{\phi_{Cu}} \cdot 100 & \text{if } \phi_{Cu} < 50\% \end{cases} \quad (11)$$

where $\phi_{steel} = 100 - \phi_{Cu}$ and $\phi'_{steel} = 100 - \phi'_{Cu}$.

It was found that the real amounts of copper in joints are systematically several percent bigger than calculated ones. This error can be explained as follows: firstly, level set method does not con-

sider the solubility limits of the materials, secondary it neglects the diffusion between the components and thirdly, with actual resolution, it is capable to recreate only bulk components of morphology, when all structures with the size lower when $50 \mu\text{m}$ are neglected.

Steel components, with the exception of Ni, has very low solubility in copper and form the precipitates in copper medium, when copper maximal solubility in austenitic structure is about 20% (under condition of rapid cooling, which is respected at the case of electron beam welding). A positive relative error of 6–16% observed for copper-rich and mixed joints can be explained, from one side by neglecting of Fe and Cr precipitation in copper medium, which quantity cannot be previewed in this model, and from the other side, by neglecting Cu solubility in austenitic structure. The negative relative error found for negative “d” can be explained by neglecting of diffusive transport, which is important for this type of morphology.

5. Conclusions

Present numerical model gives a first approximation to realistic reproduction and prognostics of morphology and composition of dissimilar welds formed between metals with limited solubility. It demonstrates the influence of operational parameters as beam position and welding speed on heat transfer and convective movements in melted pool. It gives also the possibility to obtain the morphological map of the weld, in the other words, to predict the distribution of immiscible materials at the macroscopic level.

It was demonstrated that the mixing process in melted zone is mostly determined by the proportion of melted components, which is controlled by the deflection of electron beam from joint line. The mixing pattern forms during competitive flow of two fluxes with different composition past the keyhole.

In spite of number of simplifications, which allow reducing the time of calculation, the results obtained in this modeling are in good correspondence with experimentally available data (local

Table 3

A comparison of calculated copper fraction in melted zone ϕ_{Cu} with real Cu amount.

Weld	ϕ_{Cu} (at.%)	ϕ'_{Cu} (%)	E (%)
2	91.3	81	11.4
3	95.3	83	13.3
4	94.2	82	13.2
5	94.5	89	5.8
6	8.8	5	−4.4
7	52.7	49	−7.8
8	58.2	53	8.9
9	94.1	79	15.7
10	94.7	98	3.6
11	95.1	95	0.6

composition, shape and dimensions of the welds). Three types of morphology, which can be observed experimentally, have been successfully recreated.

References

- [1] N. Chakraborty, S. Chakraborty, *Journal of Heat and Mass Transfer* 50 (2006) 1805–1822.
- [2] L. D'Alvise, E. Massoni, S.J. Walløe, *Journal of Materials Processing Technology* 125–126 (2002) 387–391.
- [3] S.M. Dörfler, Advanced modeling of friction stir welding – improved material model for aluminum alloys and modeling of different materials with different properties by using the level set method, in: *Comsol Multiphysics European Conference 2008, Hannover, 2–4 November 2008* (presentation CD).
- [4] G. Wilde, J.H. Perepezko, *Acta Materialia* 47 (1999) 3009–3021.
- [5] K. Kazemi, J.A. Goldak, *Computational Materials Science* 44 (2009) 841–849.
- [6] J. Montalvo-Urquiza, Z. Akbay, A. Schmidt, *Computational Materials Science* 46 (2009) 245–254.
- [7] Chin-Hyung Lee, Kyong-Ho Chang, *Computational Materials Science* 40 (2007) 548–556.
- [8] Nicolas Pierron, Pierre Sallamand, Simone Matteï, Numerical modeling of melted pool formation during an interaction of a pulse laser (Nd:Yag) with an aluminum sheet, in: *Proceedings of the European Comsol Conference 2005 in Paris, France* (CD of proceedings).
- [9] I. Tomashchuk, J.-M. Jouvard, P. Sallamand, Numerical modeling of copper–steel laser joining, in: *Proceedings of the European Comsol Conference, vol. 2, Grenoble, France, 2007*, pp. 615–619.
- [10] I. Tomashchuk, P. Sallamand, J.-M. Jouvard, Modeling of microstructures in dissimilar copper/stainless steel electron beam welds, in: *Comsol Multiphysics European Conference, Hannover, Germany, 2008* (presentation CD).
- [11] A. Soveja, J.M. Jouvard, D. Grevey, Metal surface laser texturing: multiphysics modelling of a single impact effect, in: *Proceedings of the European Comsol Conference, vol. 2, Grenoble, France, 2007*, pp. 641–647.
- [12] J.M. Jouvard, A. Soveja, N. Pierron, Thermal modelling of metal surface texturing by pulsed laser, in: *Proceedings of the European Comsol Conference, Paris, France, 2006* (CD of proceedings).
- [13] P. Peyre, P. Aubry, R. Fabbro, Thermal modelling and experimental validation of the manufacturing process, in: *Proceedings of the European Comsol Conference, vol. 2, Grenoble, France, 2007*, pp. 588–593.
- [14] S. Osher, J.A. Sethian, *Journal of Computational Physics* 79 (1988) 12–49.
- [15] H. Ki, P.S. Mohanty, J. Mazumder, *Journal of Physics D: Applied Physics* 34 (2001) 364–372.
- [16] A.K. Dasgupta, J. Mazumder, *Journal of Applied Physics* 102 (2007).
- [17] F.J. Vermolen et al., *Computational Materials Science* 39 (2007) 767–774.
- [18] T. Iwamoto et al., *Computational Materials Science* 44 (2008) 792–801. 793.
- [19] D. Smith, *Multiphase Flow, Comsol News, Comsol Inc., 2009* <(http://www.comsol.eu)>.
- [20] O.K. Nazarenko, *Avtomaticeskaya Svarka* 1 (1982) 33–39.
- [21] B.E. Paton, *Electron Beam Welding, Kiev, 1987*.
- [22] G. Sayegh, A. Voisin, in: *4th International Colloquium on Welding and Melting by Electron and Laser Beams, Cannes, France, September 88, Tom 1, pp. 159–166*.
- [23] I. Tomashchuk, P. Sallamand, J.M. Jouvard, Assemblage hétérogène cuivre/inox par faisceaux d'électrons, *Journée de la Fédération Française des Matériaux: Techniques d'Assemblage Pour des Conditions Extrêmes, 25–26 Septembre 2008, Nancy*.
- [24] V.R. Voller, Numerical methods for phase-change problems, in: W.J. Minkowycz et al. (Eds.), *Handbook of Numerical Heat Transfer, John Wiley, New York, 2006* (Chapter 19).
- [25] J. Crank, *Free and Moving Boundary Problems, Clarendon Press, Oxford, 1984*.
- [26] Z. Yang, PhD Thesis, The Pennsylvania State University, 2000.
- [27] E. Guyon, J.-P. Hulin, L. Petit, *Hydrodynamique Physique, Paris, 1994*.
- [28] J. He, J. Zhou Zhao, L. Ratke, *Acta Materialia* 54 (2006) 1749–1757.
- [29] J. Gnauk, R. Wenke, G. Frommeyer, *Materials Science and Engineering A* 413–414 (2005) 490–496.